受入
88-10-287
高工研図書室

EUROPEAN ORGANIZATION FOR NUCLEAR RESEARCH

CERN-EP/88-126
September 23rd, 1988

PERFORMANCE OF THE SCINTILLATING FIBRE DETECTOR IN THE UPGRADED UA2 DETECTOR

J. Alitti[2], R.E. Ansorge[1], P. Bareyre[2], G. Blaylock[3], P. Bonamy[2], C.N. Booth[3]*, J. Crittenden[2]**, R.S. DeWolf[1], J. Dupont[3], K. Einsweiler[3], C. Engster[3], J-M. Gaillard[4], K. Hultqvist[3], M. Lefebvre[1], L. Linssen[3], J-P. Meyer[2], D.J. Munday[1], J.M. Pentney[1], J.G. Rushbrooke[1], A. Stirling[2], A.R. Weidberg[3], P.S. Wells[1], D.R. Wood[3], S.A. Wotton[1], T.O. White[1] and H. Zaccone[2].

Abstract

A large scintillating fibre detector consisting of ≈60000 scintillating plastic fibres of 1 mm diameter and 2.4 m length has been used successfully as a tracking and preshower detector in the UA2 experiment at CERN. The detector readout, the pattern recognition algorithm and the results from the $\bar{p}p$ data taking run are described.

---

1) Cavendish Laboratory, University of Cambridge, Cambridge, UK.

2) Centre d'Etudes Nucléaires de Saclay, France.

3) CERN, 1211 Geneva 23, Switzerland.

4) LAL, Université de Paris-Sud, Orsay, France.

*) now at Dept. of Physics, Univ. of Sheffield, Sheffield, UK.

**) now at Physikal. Inst., Bonn Univ., Fed. Rep. of Germany.

1. INTRODUCTION

At the end of 1987, the upgraded UA2 experiment took its first data at the SPS $\bar{p}p$ collider. The upgrade of the UA2 detector [1] was designed to take advantage of the increased luminosity expected after the completion of the improvements to the CERN S$\bar{p}$pS complex at the end of 1987. Emphasis was put on improving the missing transverse energy measurement by increasing the coverage of the electromagnetic and hadronic calorimetry down to a polar angle of 6^0, and also on better electron identification. The scintillating fibre detector (SFD) [1-3] forms the outer part of a new detector, which fits inside the central calorimeter and provides tracking and electron identification. Inside the SFD are a cylindrical drift chamber, a layer of silicon pads and a transition radiation detector, which occupies half of the available radial space, leaving very little room for additional tracking and electron identification. As a result, the scintillating fibre detector was chosen as a very compact cylindrical tracking and preshower detector.

In section 2 we present the general features of the scintillating fibre detector. The image intensifier systems are described in section 3 and the operation of the CCD's and the online readout in section 4. After a description of the pattern recognition algorithm used for track reconstruction (section 5), we present the first results on the detector performance during the $\bar{p}p$ data run and cosmic ray tests (section 6). Conclusions are given in section 7. For a detailed description of the fibre detector construction and the CCD data digitisation and compaction we refer to [3] and [4] respectively.

2. GENERAL FEATURES OF THE SCINTILLATING FIBRE DETECTOR

The SFD consists of 24 layers of 1 mm diameter 2.4 m long scintillating plastic fibres ($\approx$60000 fibres in total). The active part is 2.1 m long and has a total thickness of 6 cm at an average radius of 41 cm. It covers polar angles θ from 20° to 160°. The inner 18 fibre layers (6 stereo triplets) are used as a tracking detector. They are surrounded by a 1.5 radiation length lead converter in the region of the central calorimeter ($40° < \theta < 140°$). The additional 6 layers (2 stereo triplets) outside the converter are used as a preshower detector to detect the early development of electromagnetic showers. The converter is tapered such that particles leaving the interaction vertex traverse 1.5 radiation lengths, independent of their angle. In each stereo triplet one layer of fibres is arranged parallel to the axis of the cylinder. The other two are at angles $\pm \alpha$, where $\alpha = 15.75°$ for the tracking part and $\alpha = 21°$ for the preshower part of the detector.

The fibres [3] consist of a 1 mm core of polystyrene doped with butyl-PBD and POPOP, surrounded by a 10 μm polyvinyl acetate cladding to provide internal reflection. To prevent cross talk between adjacent fibres and to improve their mechanical stability, the fibres are covered with 0.1 μm aluminium by sputtering.

They are read out from one side only and the other end is coated with reflective aluminium (ε_r = 55%) to partly compensate for the attenuation of light in the fibres ($\lambda_{att} \approx 1.65$ m). The light yield at 1.3 m distance for a minimum ionising particle passing through 1 mm fibre thickness is 23 photons of average wavelength 440 nm.

The signals from the fibres are read out and multiplexed by 32 optoelectronic systems, 16 on each side of the detector (see Fig. 1). The fibres are divided between these read-out chains according to the azimuthal angle ϕ at their read-out end. The fibre-ends of $\approx$ 2000 fibres are grouped in a non-compact rectangular array (50 × 66 mm^2) by a perforated plate and held at the input of an image intensifier chain (see Fig. 2). Each layer of fibres on the detector is split into two staggered layers on the coupling plate. The minimum distance between fibre-centres in the plate is 1.3 mm. The image intensifiers amplify the light signal and demagnify the area covered by the fibres so that the image fits onto the active area (4.3 × 5.8 mm^2) of a charge coupled device (CCD). A single CCD contains 145 × 208 photosensitive pixels. The light from each individual fibre is spread out over $\approx$ 12 CCD pixels. Online data compaction is achieved by a purpose-built FASTBUS digitiser [4]. The correspondence between the fibres of the detector and the CCD pixels is measured with the aid of 91 fiducial fibres spread uniformly over the face of each image intensifier. These fibres may be illuminated through the aluminium coating at the fibre-end opposite to the readout.

3. THE IMAGE INTENSIFIERS

Each image intensifier system[1] consists of two electrostatically focused image intensifiers (II) and one proximity focused II containing a micro channel plate (MCP) (see Fig. 3). Their basic properties are summarised in table 1. A full description of the image intensifiers and of the saturation and life-time properties of the MCP may be found in [2]. The reduction of the image by the first II is adjustable and is set to 0.2. The total reduction of the fibre image varies from 0.07 in the centre to 0.08 near the edge of the sensitive area.

Prior to installation on the detector, the response of each II system as a function of the input surface location was measured with a light source of calibrated intensity distribution. The light amplification in the II varies mainly as a function of the radius R_i on the input face. The response at the centre is typically two times higher than at the outer corners of the image (R_i = 40 mm). This is partly due to the variation of the quantum efficiency of the first photocathode which has its maximum at the centre of the image, decreases by 15% at R_i = 30 mm and increases again by 5% near R_i = 40 mm. Construction specifications required its quantum efficiency to be larger than 13% for any element of the photocathode area.

[1] Delft Electronische Producten, Roden, The Netherlands.

Table 1: Image Intensifier Parameters

	II_1	II_2	II_3
input diameter	80 mm	18 mm	18 mm
output diameter	18 mm	18 mm	7 mm
photon gain	~10	~1000	~6
cathode-anode potential	20 kV	7 kV	15 kV
photocathode	S20	S20	S20
quantum efficiency	>13%	16%	16%
phosphor	P47	P47	P46

This includes the effect that only about 70% of the area of the fibre-optic window is active for light transmission. The amplification loss due to the couplings between the different stages amounts to a factor of ≈ 1.5. The total light amplification at the centre is tuned to be ≈ 40000. It is checked regularly during data taking runs using the average pulse height observed on charged particle tracks and corrected if necessary by adjusting the MCP voltage. To prevent light entering the sensitive area of the CCD during image transfer (see next section), the second II may be gated off by making its photocathode potential less negative than the MCP entrance voltage. To monitor the photoelectronic flow in the image intensifiers, the electrical current through the last image intensifier is measured continuously. Whenever this current exceeds a threshold (typically 100 nA) an alarm is set and the MCP voltage is switched off.

The orientation of the output image and the quality of the focus depend strongly on magnetic fields. A field of 0.2 G (earth's magnetic field) parallel to the axis of the II system causes a 3° rotation of the image, of which 2/3 takes place in the first tube. The spatial point-source resolution of the II system is estimated to deteriorate by at least 30%. To avoid these effects the image intensifiers are surrounded by μ-metal shielding.

As electrons and photons produce showers containing many charged particles in the lead converter, the average light-output from the fibres in the preshower region was expected to be approximately 3 times higher than in the tracking region. To equalize ageing effects in the MCP a light attenuator was placed between the first and the second II in the region of the preshower detector. However, in the detector the measured charge ratio was found to be about 1. Due to the bias introduced by the hardware threshold (see section 4.2) this measurement underestimates the real

charge ratio by about 30%. As most of the particles leaving the $\bar{p}p$ interaction vertex have energies below 1 GeV, the observed low charge ratio is presumably due to secondary particles produced in front of the SFD being absorbed in the lead converter. Therefore the light attenuators were removed after the 1987 run.

4. THE ONLINE READOUT

The light output from each image intensifier chain is converted by a CCD into an electronic signal which is digitised by a purpose-built digitiser. The 32 digitisers are situated in two FASTBUS crates. Each crate contains an Aleph Event Builder (AEB) [5] which is used as a Read-Out Processor (ROP) for the 16 digitisers. The data from the AEBs are read out by the master event builder which collects the data from all detectors in UA2. The data are transferred from FASTBUS to the online computer via a CAMAC-to-FASTBUS interface (CFI). A general description of the UA2 data acquisition system is given in [6].

4.1 The CCD Operation

Each of the 32 CCDs[2] contains an array of about 32000 photosensitive detectors ("pixels"), of size 30 μm × 28 μm. The CCD is divided into three separate regions. The first is an image zone consisting of 145 lines by 218 columns which records the light image coming from the II chain. In each line, 208 pixels are photosensitive and 3 of the remaining pixels are used to measure the dark image level. Next to the image zone is a non-photosensitive memory zone with the same dimensions as the image zone. A row of 218 pixels, called the shift register, is adjacent to the memory zone and is used to transfer the charge in the pixels to the external electronics. The image zone contains anti-blooming electrodes which are used to make a fast clear of the image zone charge in 1 μs as described in [2]. There are no anti-blooming electrodes in the memory zone so it cannot be cleared in the same manner as the image zone.

The timing sequence of the readout is shown in Fig. 4. Antiproton-proton bunch crossings occur every 3.8 μs. If there is no first level trigger after a bunch crossing (see [6] for a description of the UA2 trigger system), a fast clear is applied to remove the charge from the sensitive area of the CCD before the next bunch crossing. If there is a first level trigger then the CCD readout is started. The IIs are gated off before the following bunch crossing for a period of $\approx$ 600 μs to prevent event pileup on the CCD during the transfer of the charge from the image zone to the memory zone. If there is a second level trigger veto (after ~ 1 ms) then the readout is aborted.

---

[2] Thomson-CSF 7852

The control of the readout for all CCDs is done by a master synchronisation board, which uses EPROMs driven by a quartz oscillator to generate programmable sequences for the CCD clock signals. Three separate programs are stored in EPROM memory. The first program performs the standard readout sequence. It generates 145 vertical transfers to shift the data from the image to the memory zone. This also has the effect of dumping the noise of the memory zone into the shift register. Therefore the shift register is cleared by applying 218 clock signals before the readout of the memory zone. After this shift register clear, the first line in the memory zone is transferred to the shift register which is then read out. This procedure is repeated 144 times to read out all the lines of the memory zone. The CCD charge transfer efficiency decreases with the shift register clock frequency and 7 MHz is the fastest frequency that can be used without degrading the resolution too much (see section 5.2). Using a 7 MHz frequency for the shift register clock, the total CCD readout time is 5.6 ms.

The clear of the shift register described in the preceding paragraph only works efficiently if the noise in the memory zone is small. If there is too much noise in the memory zone it will cause saturation in the shift register. Moreover, some of the unwanted charge will be left behind in the memory zone. This means that the first lines of the image will contain a lot of noise. The noise could be removed completely by performing a slow readout of the memory zone before the image transfer, but this would increase the readout time and thus the detector dead-time. It is therefore essential to prevent the buildup of noise in the memory zone. This is achieved by the second program, the memory zone clear, which is running between triggers to prevent the accumulation of thermal noise. It consists of a continuous free running sequence of 8 memory zone vertical transfers followed by the readout of the shift register. This clearing also ensures that any charge that has already been transferred from the image to the memory zone is removed in about 1 ms. It is automatically selected at the end of the readout or after a second level trigger veto.

The third program generates a standard CCIR TV video signal which is displayed on a TV monitor. This is used as a quick visual check of the behaviour of the II chains and to align the CCDs relative to the IIs.

The TTL logic signals generated by the synchronisation card are fanned out to 32 ECL driver modules which send balanced ECL signals to the front-end readout electronics situated directly behind the CCDs. The front-end electronics consists of two multi-layer printed circuit boards per CCD. Appropriate CCD clock signals are generated for the two phase CCD. Adjustable delay lines are used to generate the correct time delays between the two phases of each clock signal. Another system of adjustable delay lines and flip-flops generates the shift register clock and the hold signal for the track and hold amplifier which samples the CCD video output. The precise timing of the quartz oscillator is maintained by regenerating the clock signals in the front-end electronics and by using the rising edge of the clock signals. This ensures a precision of better than 1 ns. A MOS driver which is capable of driving a capacitive load and having an adjustable output voltage is used to drive the CCD

clock electrodes. However, since the capacitance of the clock electrodes changes during the edge transition of the clock cycle, it would have been better to use a voltage driver. The voltages of each CCD clock are separately adjustable. It was found that if the correct phases are maintained for each clock signal then identical voltage settings can be applied to all CCDs. The CCD itself is mounted on the second board which contains the track and hold amplifier, an analogue "black level" subtraction circuit and an amplifier with a gain of 5 as described in [2]. The video signal together with clock signals to control the digitiser timing are sent to the counting room over 80 meters of shielded twisted pair cable.

4.2 The Digitisers

In the counting room each CCD signal is received by a FASTBUS digitiser module, described in detail in [4]. In the digitiser, the CCD signal is amplified by a factor of two and digitised by an 8-bit flash analogue-to-digital converter (FADC)[3] capable of sampling at a rate of 20 MHz with a 5 MHz analogue bandwidth. Since the FADC is used after a track and hold amplifier its effective bandwidth is adequate. The FADC reference is set so that 1 ADC count corresponds to 1 mV at the output of the CCD. The digitisers also act as hard-wired processors for real-time data compaction. For normal data taking they perform the following sequence of operations:

i. Pedestal subtraction pixel by pixel.

ii. Noise compensation: The pedestal subtracted value of pixel 8 of each line (which is a non-photosensitive pixel) is subtracted from each of the subsequent pixels on the line. This removes the effects of low frequency noise or slow thermal drifts. A comparison is then made with a fixed threshold of 2 ADC counts. The noise above this threshold is negligible.

iii. Pixel-to-fibre mapping: The digitisers contain in memory a map of which pixels to assign to each fibre. The total pulse height belonging to each fibre is summed and data are output for hit fibres.

This sequence is performed in a pipelined manner, so that no additional dead-time is introduced by the data processing. By using pedestal subtraction and pixel-to-fibre mapping, the digitisers reduce the data length per event from 1.2 Mbytes to $\approx$ 30 kbytes. The total SFD read-out dead-time including the readout of the digitisers by the ROPs is about 10 ms.

---

[3] Thomson – TS8328

4.3 The Online Monitoring

During data taking a monitoring task is run on the online computer to check the integrity of the data. Any major hardware errors in the readout are detected immediately. Between normal data taking periods, special stand alone programs can be run on the ROPs:

i. Pedestals: With no beam in the SPS, events are accumulated by the ROP and the average signal in each pixel (the pedestal) is calculated and stored in a memory in the digitisers. Event by event variations are recorded to monitor the noise level. A summary file is kept so that any long term drift can be detected.

ii. Position check: The fiducial fibres are illuminated by a flasher system and their positions are calculated by the ROPs and compared with the previous positions. This procedure detects any movement of the CCDs with respect to the image intensifiers.

iii. The fiducial system is also used to obtain a quick verification of the gain of all read-out chains. The fiducials are illuminated and the average pulse height in a sample region of the CCD is measured. This procedure checks the stability of the gain of each chain to about 10%. A more precise survey of the gain of the readout chains is done offline using the average pulse height observed on charged particle tracks.

Using the position check program, it was found that there are slow drifts of the CCD relative to the IIs. It was therefore necessary to take fiducial data and recalculate pixel-to-fibre maps every week. Over this period, global shifts of the pixel-to-fibre maps were typically smaller than 0.5 pixel whereas one or two read-out systems could show shifts of up to 1 pixel.

5. THE PATTERN RECOGNITION

In this section we describe the pattern recognition algorithm used for the tracking part of the SFD. The basic algorithm is described first, followed by a section on the intrinsic resolution of the readout and the resulting refinements of the tracking code. The pattern recognition for electromagnetic clusters in the preshower detector is covered in section 6.3.

5.1 The Basic Algorithm

We use a cylindrical coordinate system (z,R,ϕ), with the beam along the z-axis and the centre of the interaction region at z = 0. When a charged particle crosses the detector it produces light in the fibres it traverses. These fibres will form a pattern of three segments (hereafter called projections) in the z = 0 plane. In general, the angular separation $\Delta\phi$ of a stereo fibre from its axial partner in this plane depends on the polar angle θ of the track, the position of the vertex z_V (assuming $x_V = y_V = 0$) and the stereo angle α:

$$\Delta\phi = \cot\theta \cdot \tan\alpha + (z_V / R) \cdot \tan\alpha \qquad (5.1)$$

The stereo fibres lie on either side of the axial fibres at equal distances. This is illustrated in Fig. 5 for an ideal track. If the track originates from a vertex at $z_V = 0$, then all three projections are radial. If the track originates at a point $x_V = y_V = 0$, $z_V \neq 0$, then the two stereo projections are tilted with respect to the axial projection. For the preshower detector the separation $\Delta\phi$ is larger because of the larger stereo angle.

The pattern of radial projections lends itself to a histogramming technique for track-finding. Searching through a histogram of the ϕ-coordinates of hit fibres locates the track projections. Small corrections to the stereo layers can accommodate the slightly non-radial projections coming from vertices displaced from z = 0. The final 3-dimensional track candidates are then built out of triplets of projections in which the two stereo projections are at equal distances from the axial projection, on opposite sides (referred to as the symmetry requirement).

The first step of the technique is to construct the ϕ-histogram of hit fibres for each of the three stereo angles. For a given fibre angle, the hit fibres in the six layers of interest are entered into a histogram whose bin size is approximately equal to a fibre diameter. The histogram contains a 6-bit word for each ϕ-bin, telling which of the six layers have been hit.

When the vertex is not located at $z_V = 0$, the ϕ-coordinates of stereo hits are corrected according to equation 5.1. An accuracy of 10 cm in the vertex position is sufficient for this correction and the necessary information is provided by a fast SFD vertex finder. The vertex finder makes use of equation 5.1 by looking at the multiplicity of radial projections observed in the stereo layers as a function z_V. This method measures the z-coordinate of the interaction vertex with an accuracy of 35 mm (rms). For the 1988 run, a fast determination of the vertex with a precision better than 1 mm will be provided by the combination of two layers of silicon pad counters, one at R = 14 cm and a new detector at R = 3 cm [7].

The process of finding projections involves scanning each histogram for bins in which several layers are occupied. At least three hit layers per projection are required. Because of the imperfect positioning of fibres in the detector and because

of binning effects inherent to the technique, it is necessary to look for projections within a window of 3 bins in order to be fully efficient. Fibre hits which are shared by adjacent projections are assigned only to the projection with the highest pulse height. This algorithm resolves all projection overlaps while preserving the longest and brightest projections.

The result of the histogram scan is a list of track projections and the hit fibres contributing to each. A straightforward search for triplets of projections which satisfy the symmetry requirement produces a list of all possible track candidates.

5.2 The Intrinsic Resolution of the Readout System

The correspondence between the fibres of the detector and the CCD pixels is measured using the fiducial fibres. The measured CCD positions of the 91 fiducial fibres in each read-out system are compared with their expected positions in a fitting routine which describes the absolute alignment, reduction and distortion of the image. The 20-parameter fit reproduces the fiducial fibre positions to about 0.3 pixels (rms). This corresponds to 0.13 mm at the II input. Using the results of the 32 fits, the CCD positions of all fibres in the detector are stored in the pixel-to-fibre maps, which are used by the FASTBUS digitisers for online data compaction.

Each layer of fibres in the detector is split into two staggered layers on the coupling plate. The minimum distance between fibre centres is 1.64 mm for fibres in the same layer of the coupling plate and 1.3 mm for fibres in adjacent layers (see Fig. 2). The finite resolution of the optoelectronic readout causes a fraction of the light emitted by a fibre to be detected outside the pixels assigned to that fibre. This effect was studied using fitted tracks in the detector. Fig. 6 displays the fraction of the produced light which is assigned to the correct fibre, as well as the fraction assigned to the 6 nearest neighbours on the coupling plate. On average, 78% of the signal is detected in the pixels which are mapped to the central fibre and 1.5% is detected in the fibre opposite to the read-out direction. At 7 MHz readout frequency 5% is detected in the fibre along the read-out direction. This fraction decreases to 3.5% at 4 MHz. The other 4 fibres detect on average 4% of the signal each. Converting these numbers to the spatial resolution for a point source illuminating the input of the first image intensifier gives an effective rms of 33 μm at the input of the CCD. However, the above fractions are biased by the online pixel threshold of 2 ADC counts and the real spatial resolution is estimated to be about 40 μm.

Due to this smearing effect, the number of data words after online pixel-to-fibre mapping in the FASTBUS digitisers is substantially higher than the number of fibre-signals from the detector. Moreover it introduces many ambiguities. To overcome these problems a simple algorithm has been implemented in the ROPs which clusters together adjacent fibres in the same fibre layer if they are not separated by at least two consecutive fibres with lower pulse height. The algorithm operates on events already buffered in the ROP, thus it does not introduce

additional dead-time. It is completed in about 50 ms and reduces the average SFD data size by a factor 2.

5.3 Refinements of the Tracking Algorithm.

The online algorithm only clusters hits within the same fibre layer in the detector and does not correct for light leaking into pixels which belong to a different fibre layer. As a result, some fake fibre hits remain and, because of the layout of the fibres on the coupling plate, these fake hits tend to form segments in the $z = 0$ plane, which are capable of mimicking a projection. However, these fake projections tend to be non-radial, they have fewer layers hit and they have a much lower pulse height than real projections. A pulse height cut of 0.17 MIP removes about 75% of the fake projections while losing less than 1% of the real projections.

Apart from fake projections there are additional sources of ghost tracks. Studies of track candidates which don't point to the primary vertex indicate that there are roughly as many secondary particles and conversion products detected in the SFD as there are primary tracks. Moreover, there are "accidental overlaps" which result from the combination of three projections from two or three different particles and which accidentally satisfy the symmetry requirement for a track candidate. The number of accidental overlaps depends highly on the charged particle multiplicity of the event and can often approach twice the primary particle multiplicity which is on average about 13 within the SFD acceptance. A large reduction in the number of track candidates is achieved when the SFD information is combined with the information from the silicon detector [1]. The remaining fraction of spurious tracks depends on the event topology. It is less than 1% for minimum bias events.

6. PERFORMANCE OF THE DETECTOR

The performance of the detector has been monitored both in test conditions with a cosmic ray trigger and during $\bar{p}p$ collider operation. Data from $\bar{p}p$ interactions were taken during November and December 1987, corresponding to an integrated luminosity of 46 nb^{-1}. Cosmic ray data were taken during the spring of 1988 with a 1.5 m long trigger counter inserted in the beam pipe. As the UA2 detector is located 60 m below the earth's surface, the observed cosmic rays originate from muons which are primarily vertical. Requiring two back-to-back reconstructed track segments in the SFD provides a clean sample of about 8000 cosmic ray events.

6.1 Pulse Height and Detection Efficiency

Fig. 7a shows the pulse height observed on cosmic ray tracks as a function of the distance along the fibre between the track impact and the II chain input. Unlike the tracks from $\bar{p}p$ interactions, the cosmic ray tracks selected always have a near to perpendicular impact on the fibre-layers and the average fibre thickness traversed does not depend on the z-coordinate along the beam line. The solid curve shows the attenuation curve obtained from radioactive source measurements performed at the time of detector construction [3]. The dotted curve gives the corresponding pulse heights for tracks from $\bar{p}p$ interactions taking into account the incident angle and assuming the interaction vertex at the centre of the detector.

Fig. 7b shows the single fibre detection efficiency for cosmic rays as a function of the distance to the readout. The detection efficiency is determined by comparing the number of track projections with 6 layers hit to those with 5 layers hit (open circles in Fig. 7b). The same can be done by comparing 5 hits to 4 hits (full circles in Fig. 7b). The data show a detection efficiency of 84% at the centre of the detector where the $\bar{p}p$ track pulse height is a minimum. The detection efficiency is dominated by Poisson statistics in the number of photoelectrons produced at the first photocathode. It depends only weakly on the MCP gain. From a convolution of Poisson statistics and the circular cross-section of the fibres one calculates that a detection efficiency of 84% corresponds to 2.3 photoelectrons produced on average at the first photocathode for a charged particle traversing a fibre at $\theta = 90°$ and 1.3 m from the readout. This corresponds to 18 photons reaching the input of the readout for an effective quantum efficiency of 13%. The expected detection efficiency for $\bar{p}p$ data is deduced from the efficiency measurement with cosmic rays by taking into account the effect of the incident angle on the pulse height ($\propto \sin\theta^{-1}$) as was done above. The result is shown by the curve in Fig. 7b.

For $\bar{p}p$ data the track reconstruction efficiency is measured using the silicon and preshower detectors. Each hit silicon pad ($R\Delta\phi = 40$ mm at $R = 140$ mm, and $\Delta z = 8.7$ mm) is connected with the reconstructed interaction vertex. The resulting track has to be confirmed by a track segment in the preshower part of the SFD. One then checks whether a track segment is found in the tracking part of the SFD. When demanding at least 4 hits out of 6 for all three stereo projections, the average efficiency for finding the track is 91%. When one requires only 3 hits per stereo projection the tracking efficiency goes up to 96%. Both numbers are consistent with an average detection efficiency of 88% per fibre layer.

Fig. 8 shows the pulse height distribution of reconstructed tracks in the tracking part of the SFD. The pulse heights have been corrected for the attenuation of the light in the fibres (see Fig. 7a) and for the fibre-thickness traversed ($\propto \sin\theta^{-1}$). The average of the distribution is defined as 1 MIP and corresponds to 61 ADC counts per fibre spread over 12 CCD pixels on average, whereas the CCD noise is typically 0.35 ADC counts per pixel. The FWHM corresponds to 0.5 MIP.

6.2 Position Resolution

Fig. 9 shows the distribution of the distance between the coordinates measured in the individual layers and the fitted track segment. The distance is measured perpendicular to the fibres in the 18 layers of the tracking detector. The superimposed curve is the result of a fit to a Gaussian distribution giving $\sigma = 0.39$ mm. This is obtained after the offline alignment of the detector, in which the offsets and stereo angles were adjusted for each of the 768 ribbons of $\approx$ 80 fibres [3]. Corrections were also applied for the fibres that were incorrectly placed in the coupling plates (1.5% of all fibres).

The position accuracy of the SFD is also reflected in the quality of the match between the ϕ-coordinates of the hits which together form a reconstructed track:

$$\Delta\phi = (2\phi^a - \phi^+ - \phi^-) / \sqrt{6},$$

where ϕ^a, ϕ^+ and ϕ^- are the average ϕ-coordinates in the axial, stereo-positive and stereo-negative projections respectively. Fig. 10 shows the distribution of $R{\cdot}\Delta\phi$ both for minimum bias data and for cosmic rays. The FWHM of the distribution for $\bar{p}p$ data is 0.6 mm. The tails of this distribution originate mainly from tracks where one of the ϕ-coordinates is badly measured due to the proximity of another track segment. Given the event multiplicity this has a high probability to occur (about 8% of the total).

The intrinsic resolution for a 3-dimensional SFD track segment is about 0.15 mm in $R\phi$ and about 0.65 mm in z. However, when connecting this track segment to the hits in the other central detectors, the precision is dominated by multiple scattering, which amounts to $\sigma = 1.5$ mm between the interaction vertex and the SFD for 500 MeV/c particles. The 2-track resolution of the SFD is determined mainly by the online clustering algorithm, which allows tracks separated by at least 3 mm to be distinguished.

6.3 Performance of the Preshower Detector

The purpose of the preshower detector is to recognize electromagnetic showers from their charge deposition and to measure the starting point of these showers accurately. By requiring a good match between the observed track in the tracking part and the centroid of the electromagnetic cluster in the preshower part one significantly reduces the background due to charged hadrons accompanying nearby photons in the electron sample.

Fig. 11a recalls the results of SFD testbeam studies [2]. It shows the pulse height distribution for 40 GeV pions and 40 GeV electrons in the preshower part of the SFD (note the logarithmic abscissa). The distributions have been scaled by the average pulse height for a 160 GeV muon (1 MIP). The average charge deposition

for a 40 GeV electron is 20 times that of a 40 GeV pion. When a cut is set at 2 MIP the detection efficiency is only 7.3% for a 40 GeV pion, while it is 98.4% for a 40 GeV electron and 96.3% for a 10 GeV electron. The average signal profile of electromagnetic clusters in the SFD is approximately 2 times wider than that of charged particles, and its pulse height density is 10 times higher [2].

Electromagnetic clusters generally cover 10-15 fibres per layer in the preshower detector and their shape is often asymmetric and non-contiguous due to shower development fluctuations. Therefore, a clustering algorithm is used which first smears out the detected pulse heights over neighbouring fibres and then collects all charges larger than 0.04 MIP. A search is made for maxima above a threshold of 0.1 MIP. If two neighbouring maxima are more than 5 fibres apart and if the minimum pulse height in between is lower than half the pulse height of the lowest peak, the cluster is split into two. For each layer-pair with the same stereo angle the observed clusters are combined and these combined clusters are matched in space. Pulse heights are corrected for light attenuation and the particle impact angle, and a pulse height cut is made at 2 MIP.

As an illustration of the operation of the preshower detector during the $\bar{p}p$ run, we show the information from a test sample of ten $W^{\pm} \rightarrow e^{\pm}(\bar{\nu})$ decays and one $Z^0 \rightarrow e^+e^-$ decay. To select the W-candidates we require an electromagnetic energy deposition above 15 GeV in the central calorimeter. Cuts are applied to the lateral and longitudinal dimensions of the electromagnetic cluster in the calorimeter. Additional cuts reject background due to beam halo. The transverse mass of the events is required to be above 50 GeV/c^2 [8]. A search is made in front of the calorimeter cluster for clusters in the preshower detector with a pulse height above 2 MIP. These preshower clusters are required to match with a reconstructed track within $\pm$ 4 mm in Rϕ and $\pm$ 10 mm in z.

The preshower pulse height distribution for the 12 electron candidates is shown in Fig. 11b, together with the pulse height distribution for 40 GeV pions from the testbeam. It agrees with the distribution for 40 GeV electrons of Fig. 11a. Fig. 12a shows the distribution of the distance in Rϕ between the preshower cluster and the reconstructed track. The rms of the distribution is 0.6 mm. The precision in z is expected to be about a factor 3 worse due to the stereo angles. The rms of the distribution of the distance in z, shown in Fig. 12b, is 3.2 mm.

Fig. 13 shows how the electron is detected in the SFD for one of the W-candidates. The hit fibres are displayed in the z = 0 plane. A track is observed in the tracking part comprising at least 4 hits per projection. The stereo projections lie symmetrically around the axial projection. In the preshower detector one observes clusters of several fibres in each of the 6 layers. The summed pulse height of the cluster is 25 times the average pulse height for a minimum ionising particle. The distance between the centroid of the cluster and the position of the extrapolated track amounts to 0.1 mm in Rϕ and 0.9 mm in z.

7. CONCLUSION

The UA2 scintillating fibre detector operated successfully during the first $\bar{p}p$ data taking run in 1987. The position resolution of the tracking part of the detector is 0.39 mm (rms) per layer. The detection efficiency varies between 84% and 97% per layer depending on the track angle and impact position. The average track reconstruction efficiency in the SFD is 96%. In the preshower detector the average pulse height for a 40 GeV electron is 20 times that of a 40 GeV pion. The match between the position of the electron shower and the extrapolated track position is close to 1 mm in $R\phi$ and 3 mm in z and is used to distinguish between an electron and a charged hadron with a nearby photon.

Acknowledgements

It is a pleasure to thank our UA2 colleagues for their constant support and understanding. Many individuals have contributed to the realisation of the detector and we gratefully acknowledge the help from the technical staffs of Saclay, Cambridge and the EP and EF divisions at CERN.

REFERENCES

1. UA2 Collaboration. C.N. Booth, Proc. 6th Topical Workshop on Proton-Antiproton Collider Physics, Aachen, 1986, eds. K. Eggert et al., (World Scientific, Singapore, 1987) 381.
   Proposal to improve the performance of the UA2 detector, CERN/SPSC 84-30 (1984).
   Proposal to improve the performance of the UA2 central detector, CERN/SPSC 84-95 (1984).
2. R. Ansorge et al., Nucl. Instr. and Meth. A265 (1988) 33-49.
3. J. Alitti et al.,DPhPE 88-06, Centre d' Etudes Nucléaires de Saclay, 91191 Gif-sur-Yvette; The Design and Construction of a Scintillating-fiber Tracking Detector, to be published in Nucl. Instr. and Meth.
4. S.G. Katvars et al., Cavendish Laboratory, University of Cambridge, Cambridge; A FASTBUS Digitiser for the UA2 Scintillating Fibre Detector, submitted to Nucl. Instr. and Meth.
5. A. Marchioro et al., IEEE Trans. Nucl. Science 34 (1986) 133-136.
6. G. Blaylock et al., The UA2 Data Acquisition System; and, P. Baehler et al., The XOP Trigger Processor Integrated into the UA2 Data Acquisition System; Proceedings of the International Conference on the Impact of Digital Microelectronics and Microprocessors on Particle Physics, Trieste, March 28-30 1988.
7. Proposal for the installation of a second silicon array in the UA2 detector, CERN/SPSC 87-14 (1987).
8. R. Ansari et al., Phys. Lett. B186 (1987) 440-451.

FIGURE CAPTIONS

1. The geometry of the scintillating fibre detector. The orientation of the fibre layers and the arrangement of the read-out chains are shown.

2. The geometry of the plate that couples $\approx$ 2000 fibres to a read-out chain. Each layer of fibres on the detector is distributed over 2 staggered layers in the plate.

3. The image intensifier system.

4. Timing diagram showing the CCD read-out sequence.

5. Representation of an ideal track in the SFD. The hit fibres are drawn in the $z = 0$ plane. The fibre radii are scaled up by a factor 3 for clarity.

6. The effect of the finite resolution of the read-out chain on the detected signals. The hit fibre is displayed together with its 6 nearest neighbours in the coupling plate. The numbers indicate the fraction of the pulse height detected in each of the fibres.

7. a) The average pulse height observed on cosmic ray tracks as a function of the distance between the particle impact and the readout. The solid curve represents the average attenuation curve measured at the time of detector construction. The dotted curve displays the corresponding pulse heights for tracks from $\bar{p}p$ interactions taking into account the particle impact angle.
   b) The detection efficiency per fibre layer for cosmic rays as a function of the distance to the readout. The curve shows the expected detection efficiency for tracks from $\bar{p}p$ interactions.

8. The pulse height distribution for reconstructed tracks in the SFD tracking part.

9. The distance between the fitted track segment and the coordinates measured in the 18 layers of the tracking part. The superimposed curve is the result of a fit to a Gaussian distribution giving $\sigma = 0.39$ mm.

10. The match $R{\cdot}\Delta\phi$ between the three stereo projections for reconstructed tracks as described in the text.

11. a) The preshower pulse height distribution of 40 GeV pions and 40 GeV electrons as measured at a test beam.
    b) The pulse height distribution of 40 GeV pions as in a), together with the pulse height distribution of 12 electron candidates from a test sample of selected $W^{\pm}$ and Z^0 decays.

12. Components of the distance between the centroid of the cluster observed in the preshower detector and the extrapolated track for the 12 electron candidates, a) in $R\phi$, b) in z.

13. The detection of an electron in the SFD. The hit fibres are displayed in the $z = 0$ plane with their radius enlarged by a factor three for clarity.

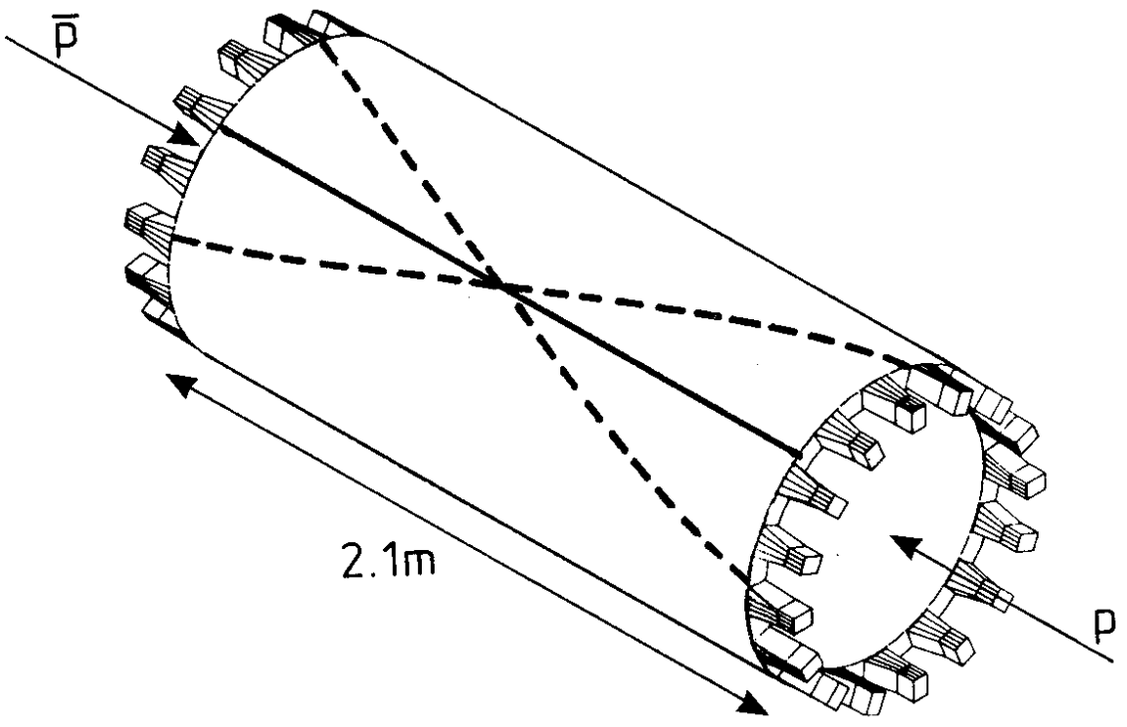

Fig. 1

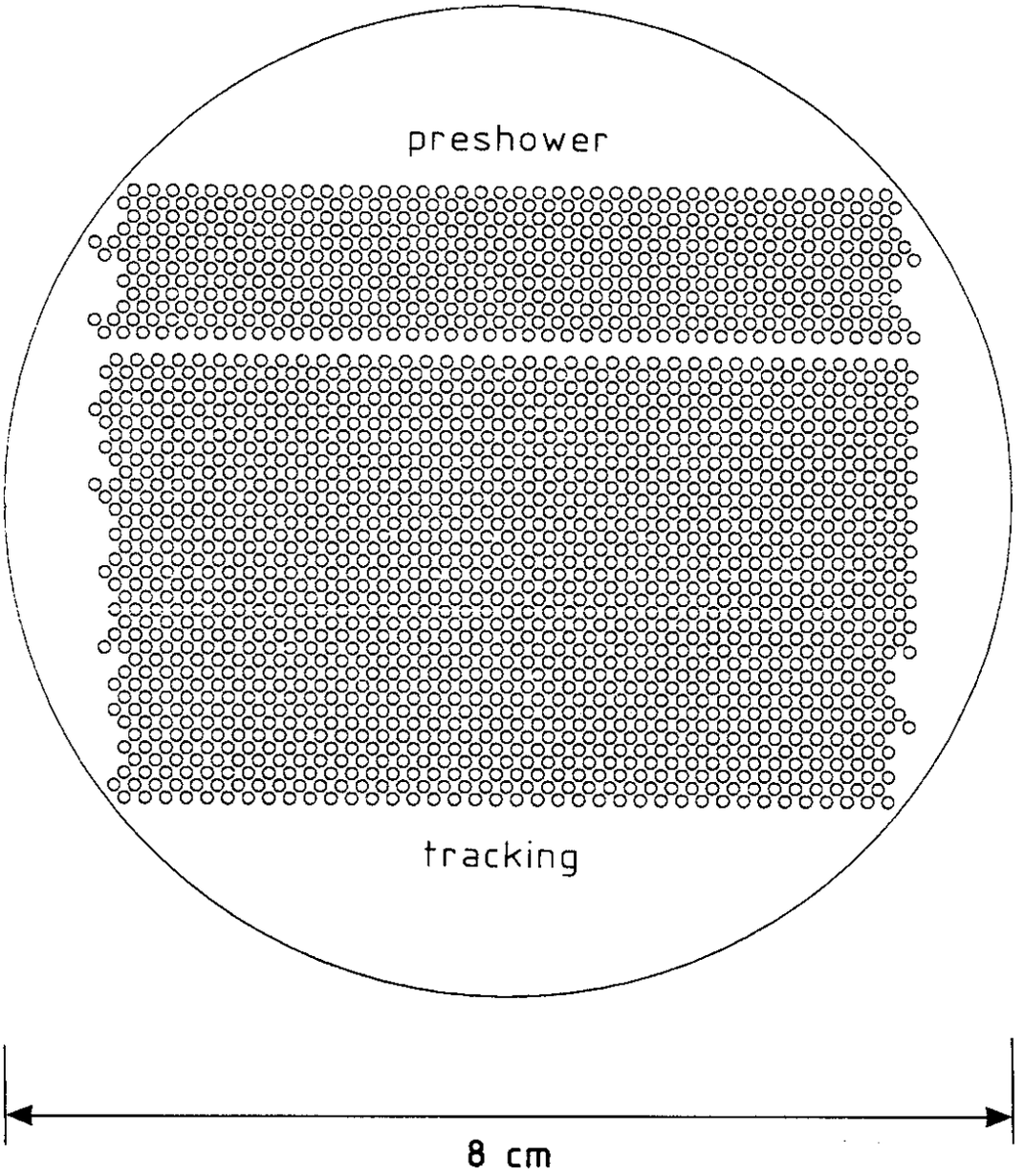

Fig. 2

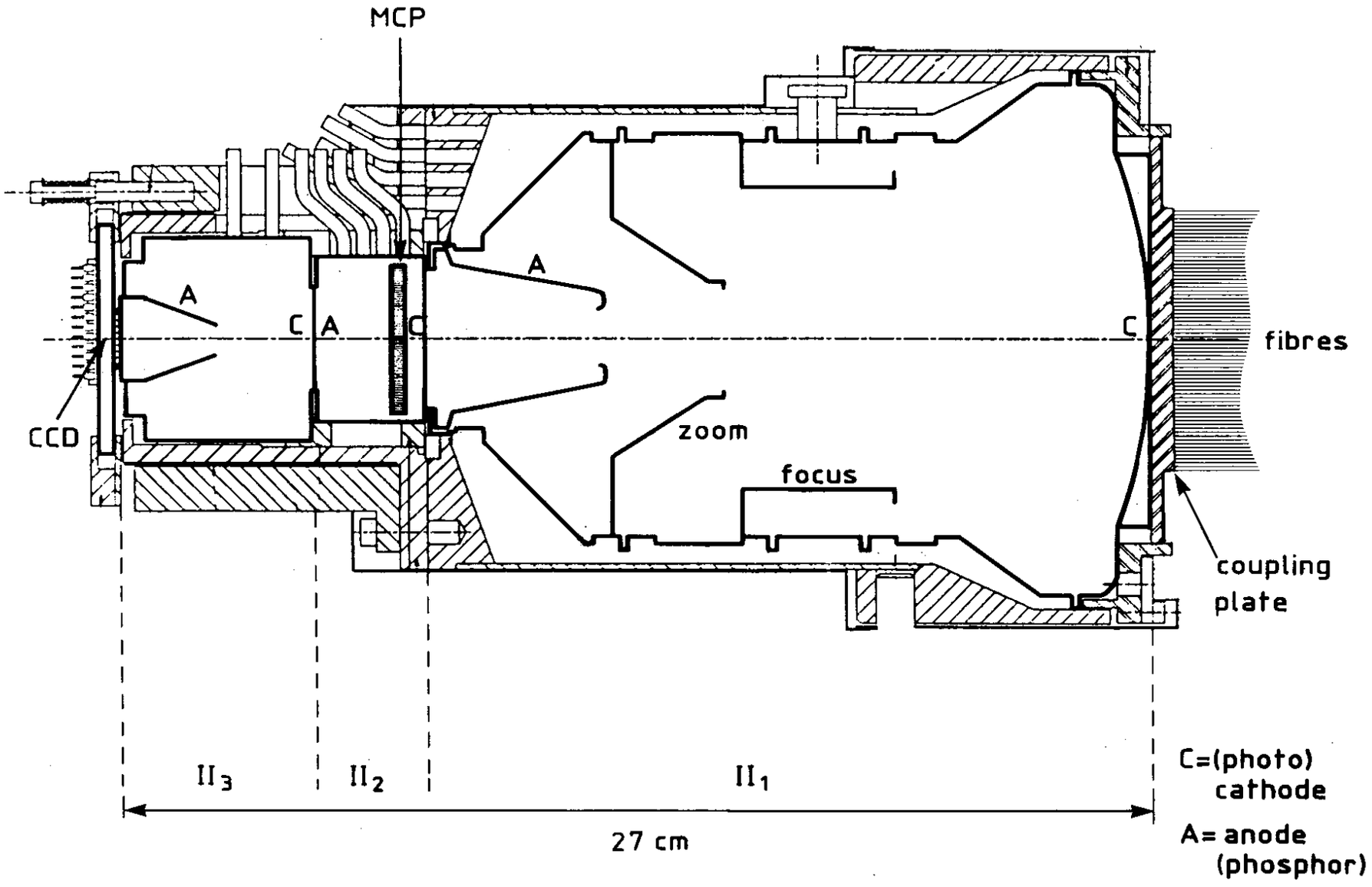
MCP
A
C
A
C
A
C
fibres
CCD
zoom
focus
coupling
plate
II3
II2
II1
27 cm
C=(photo)
cathode
A= anode
(phosphor)

Fig. 3

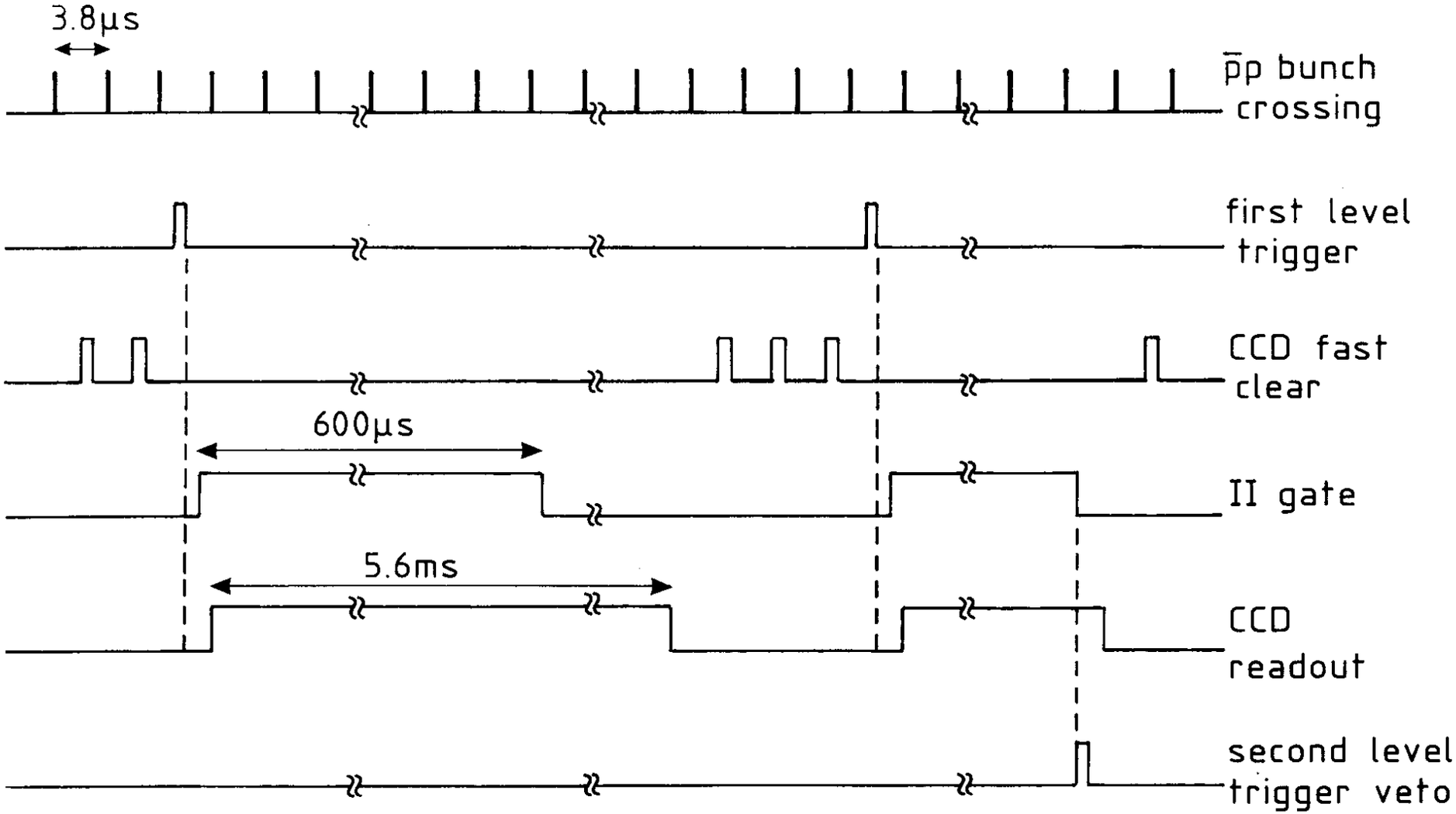
3.8μs
p̄p bunch crossing
first level trigger
CCD fast clear
600μs
II gate
5.6ms
CCD readout
second level trigger veto

Fig. 4

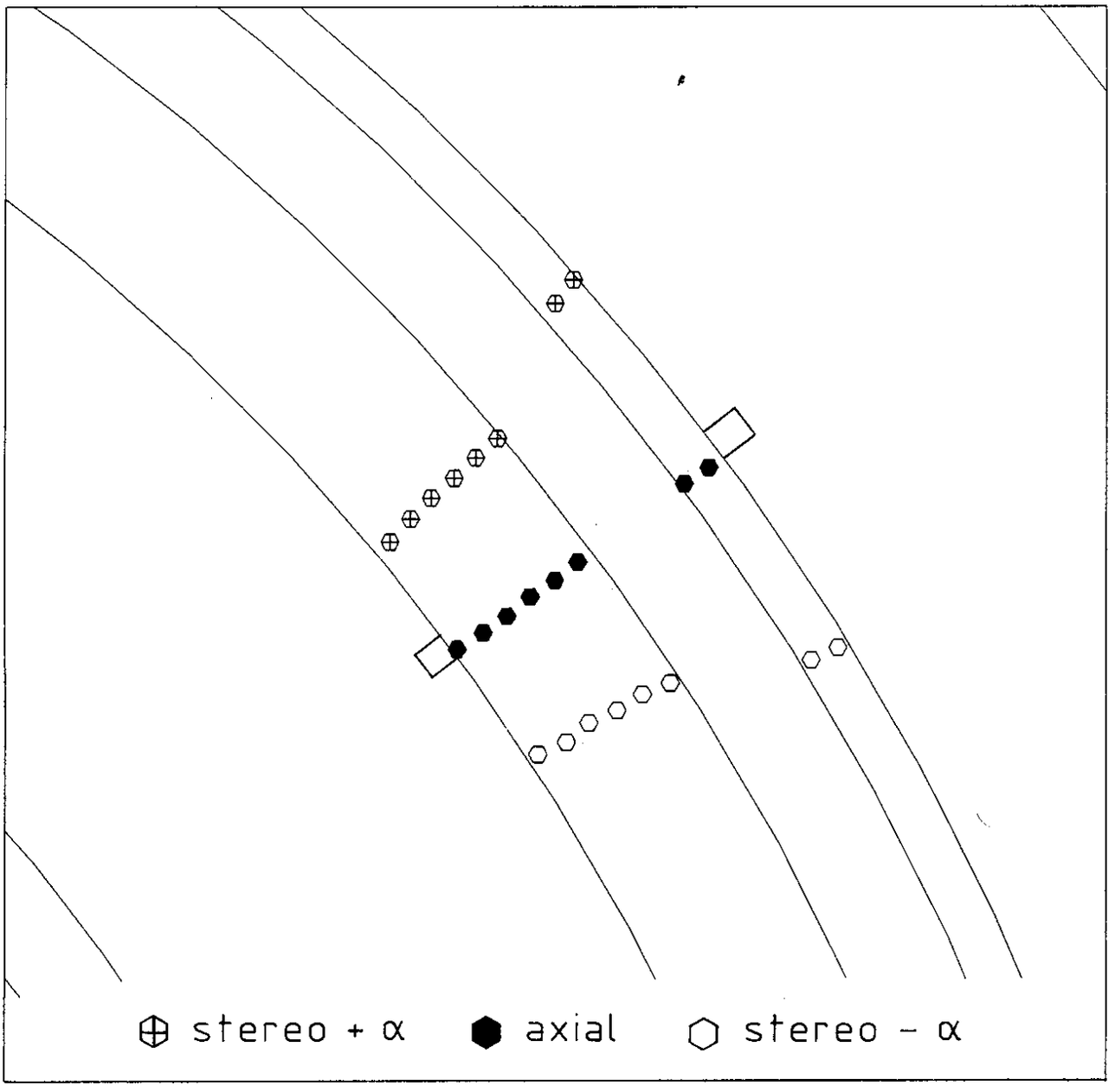

Fig. 5

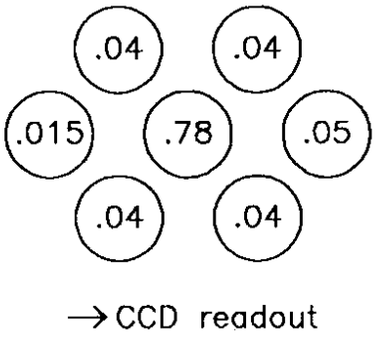

Fig. 6

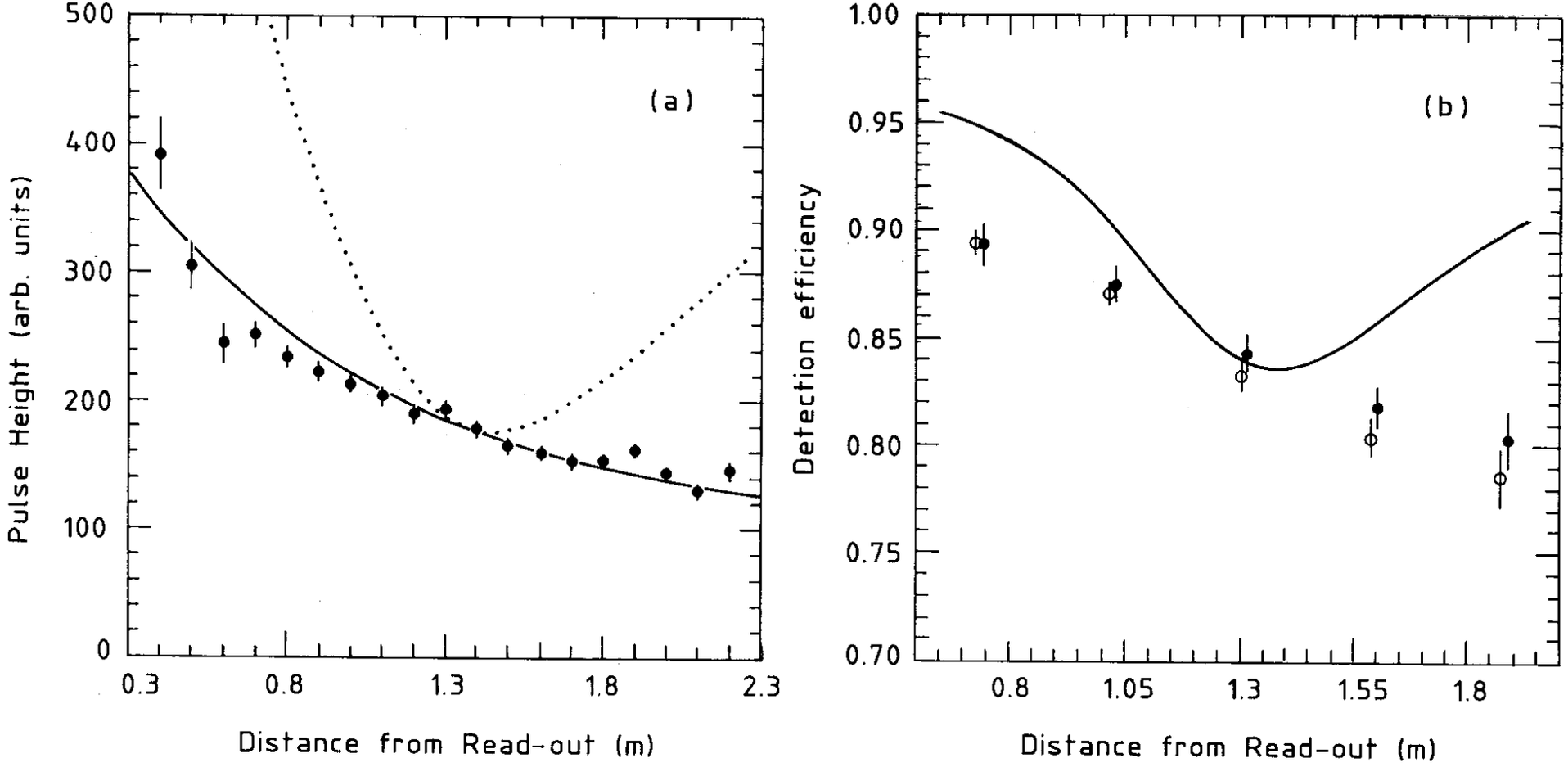
(a)
Pulse Height (arb. units)
500
400
300
200
100
0
0.3
0.8
1.3
1.8
2.3
Distance from Read-out (m)
(b)
Detection efficiency
1.00
0.95
0.90
0.85
0.80
0.75
0.70
0.8
1.05
1.3
1.55
1.8
Distance from Read-out (m)

Fig. 7

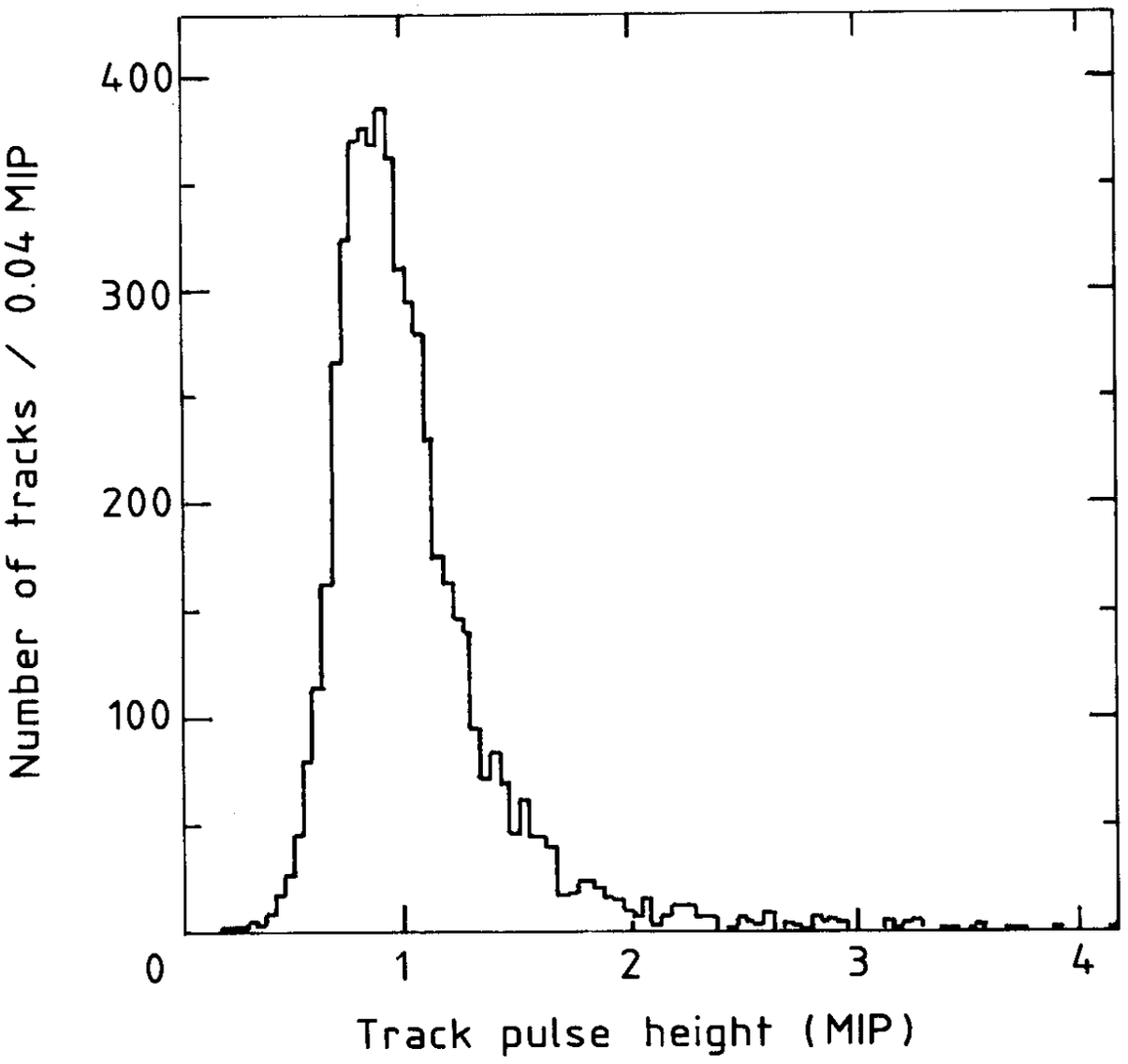
Number of tracks / 0.04 MIP
400
300
200
100
0
1
2
3
4
Track pulse height (MIP)

Fig. 8

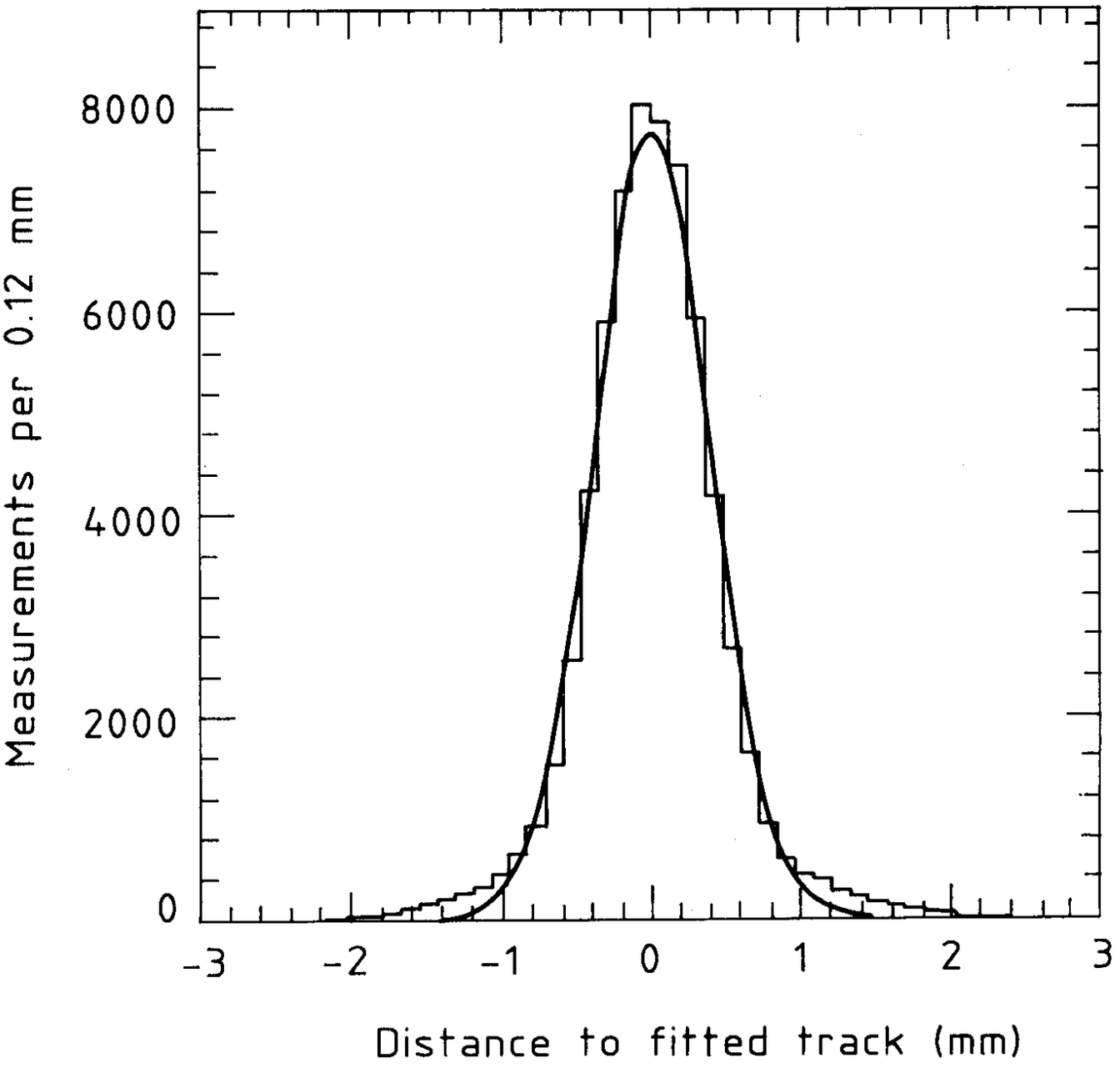
8000
6000
4000
2000
0
Measurements per 0.12 mm
-3
-2
-1
0
1
2
3
Distance to fitted track (mm)

Fig. 9

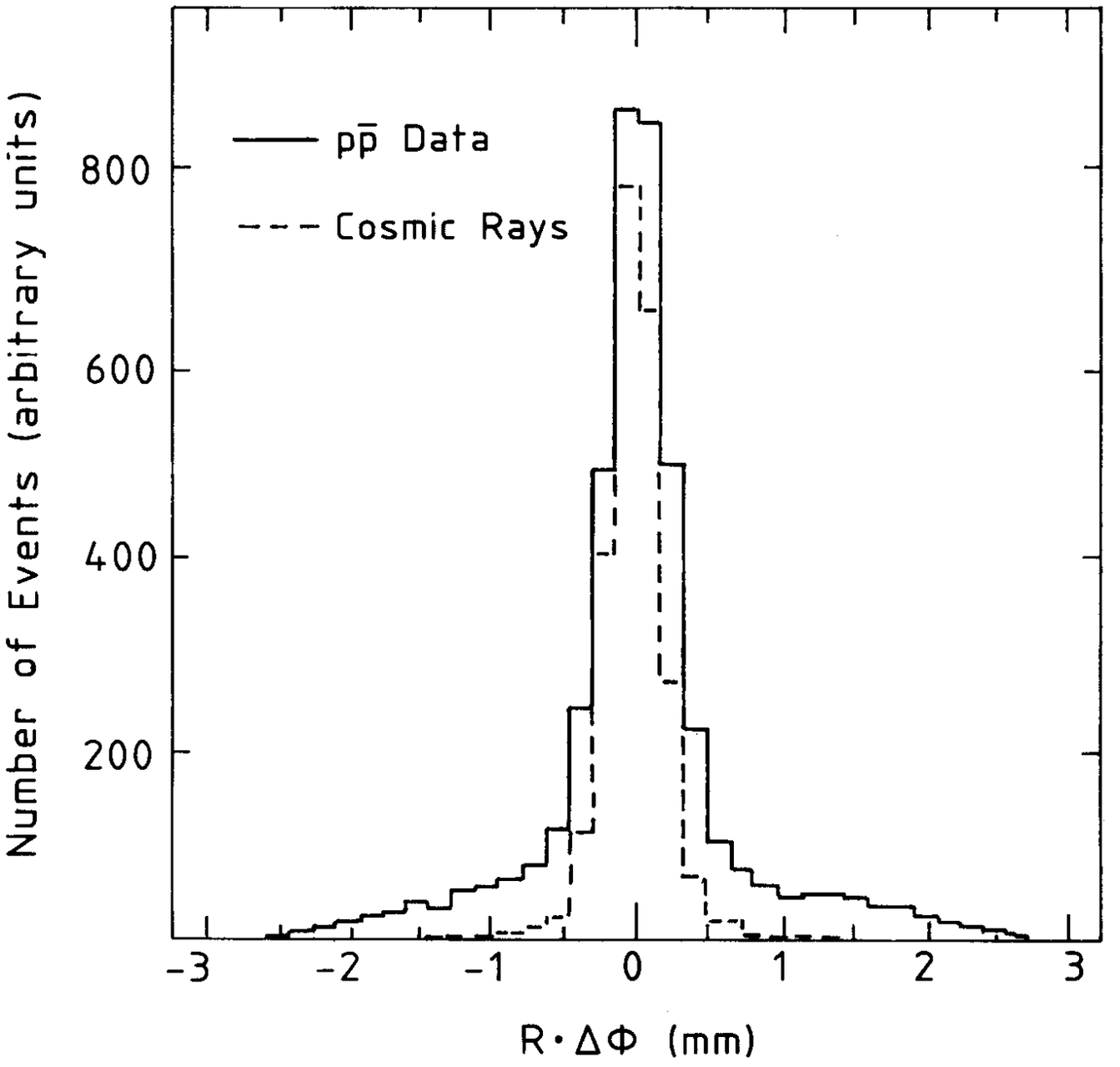
Number of Events (arbitrary units)
800
600
400
200
p$\bar{p}$ Data
Cosmic Rays
-3
-2
-1
0
1
2
3
R·ΔΦ (mm)

Fig. 10

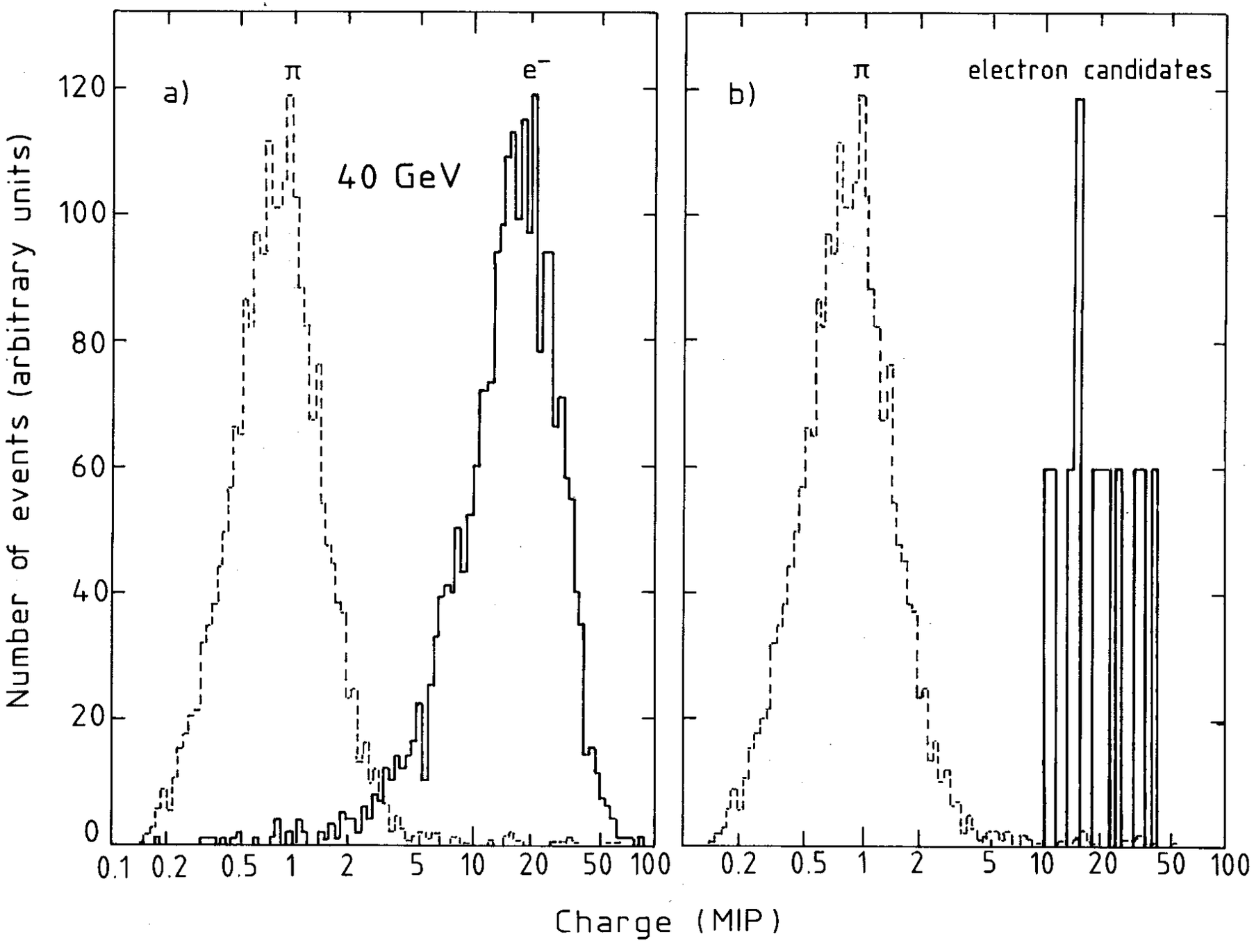
a)
π
e⁻
40 GeV
b)
π
electron candidates
Number of events (arbitrary units)
0
20
40
60
80
100
120
0.1
0.2
0.5
1
2
5
10
20
50
100
Charge (MIP)

Fig. 11

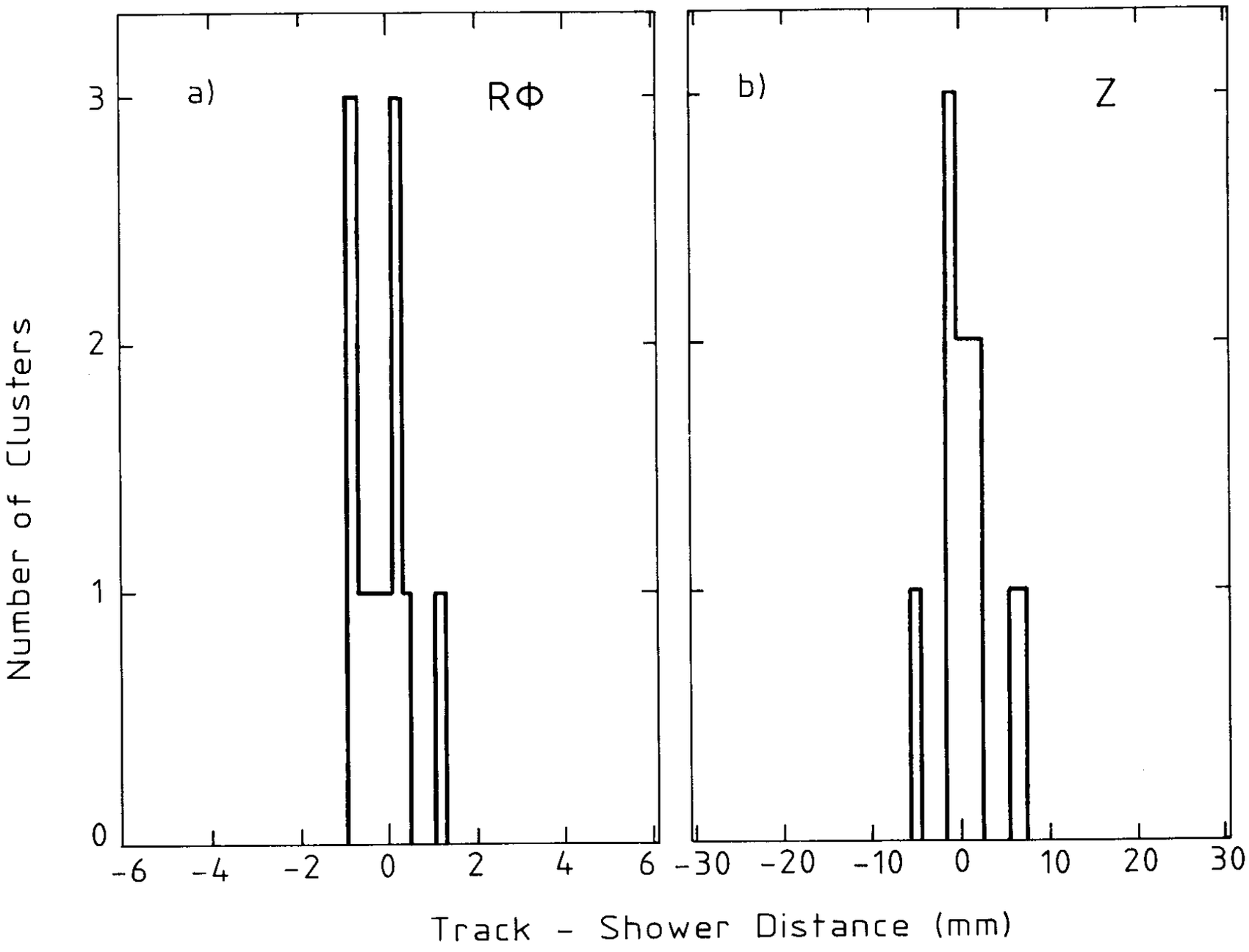
a)
RΦ
b)
Z
Number of Clusters
0
1
2
3
-6
-4
-2
0
2
4
6
-30
-20
-10
0
10
20
30
Track - Shower Distance (mm)

Fig. 12

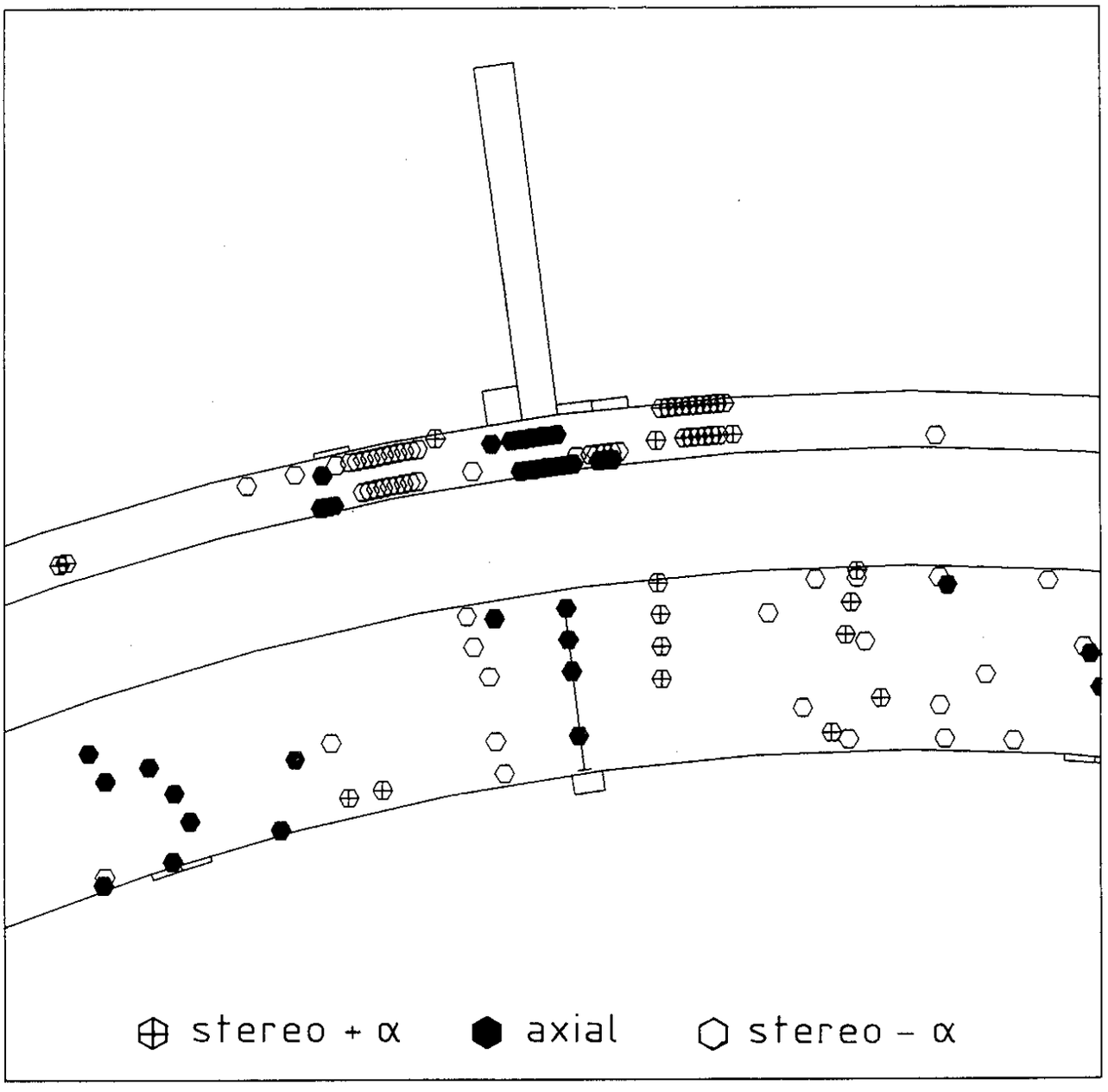

Fig. 13